



HAL
open science

Suspended sediment concentration field quantified from a calibrated MultiBeam EchoSounder

Guillaume Fromant, Nicolas Le Dantec, Yannick Perrot, France Floc'H, Anne
Lebourges-Dhaussy, Christophe Delacourt

► **To cite this version:**

Guillaume Fromant, Nicolas Le Dantec, Yannick Perrot, France Floc'H, Anne Lebourges-Dhaussy, et al.. Suspended sediment concentration field quantified from a calibrated MultiBeam EchoSounder. Applied Acoustics, 2021, 180, pp.108107. 10.1016/j.apacoust.2021.108107 . hal-03271776

HAL Id: hal-03271776

<https://hal.science/hal-03271776v1>

Submitted on 12 Aug 2021

HAL is a multi-disciplinary open access archive for the deposit and dissemination of scientific research documents, whether they are published or not. The documents may come from teaching and research institutions in France or abroad, or from public or private research centers.

L'archive ouverte pluridisciplinaire **HAL**, est destinée au dépôt et à la diffusion de documents scientifiques de niveau recherche, publiés ou non, émanant des établissements d'enseignement et de recherche français ou étrangers, des laboratoires publics ou privés.



Distributed under a Creative Commons Attribution 4.0 International License



Suspended sediment concentration field quantified from a calibrated MultiBeam EchoSounder



Guillaume Fromant^{a,b,*}, Nicolas Le Dantec^{a,c}, Yannick Perrot^d, France Floc'h^a, Anne Lebourges-Dhaussy^d, Christophe Delacourt^a

^aInstitut Universitaire Européen de la Mer, Laboratoire Géosciences Océan – UMR 6538, Rue Dumont d'Urville, 29280 Plouzané, France

^bLaboratoire d'Informatique Signal et Image de la Côte d'Opale, 50, rue Ferdinand Buisson, 62228, Calais, France

^cCentre d'Etudes et d'expertise sur les Risques, l'Environnement, la Mobilité et l'Aménagement, DTecEMF, 134 Rue de Beauvais, 60280 Margny-lès-Compiègne, France

^dInstitut de la Recherche pour le Développement, Laboratoire de l'Environnement MARin - UMR 6539, Pointe du Diable, 29280 Plouzané, France

ARTICLE INFO

Article history:

Received 20 November 2019

Received in revised form 30 March 2021

Accepted 6 April 2021

Available online 21 April 2021

Keywords:

Acoustic backscattering

Multifrequency acoustics

Suspended sediments concentration

Acoustic inversion

MultiBeam EchoSounder

ABSTRACT

Acoustic scattering can be used to estimate Suspended Sediment Concentration (SSC) through acoustic inversion methods. Current SSC quantification methods are mostly unable to observe both spatial and temporal variations. Here, we assess the possibility to measure both using a Multibeam Echosounder (MBES). MBES combine a large spatial covering in the water column and the capability to measure 'on route', allowing a better representativity of the measurements. Time-series of raw EM3002-MBES data at 300 kHz were acquired during a 5-hours field experiment at a fixed location in the Aulne macrotidal estuary (France) during ebb, ensuring sufficient SSC variations. Concurrently, 4-frequencies Acoustic Backscattering System (ABS) profiles were acquired in the water column, as well as turbidity profiles, further converted into SSC using collected water samples. An original in-situ calibration was performed on the MBES, using a tungsten sphere of known properties, which allowed corrections to be made to the volume backscattered levels over the echosounder fan. Using ABS-derived equivalent radii, the MBES backscattered signal was inverted to retrieve an SSC estimate. Good consistency between MBES time-series observations and turbidity-derived SSC is observed. This experiment demonstrates the potential use of MBES for 3-dimensional turbidity observations in coastal areas, which is of great interest for sediment flux quantification.

© 2021 The Authors. Published by Elsevier Ltd. This is an open access article under the CC BY-NC-ND license (<http://creativecommons.org/licenses/by-nc-nd/4.0/>).

1. Introduction

Suspended Particulate Matter (SPM) is ubiquitous in oceans and rivers. The study of SPM distribution and transport is essential, for SPM can impact the environment, from marine habitats and water quality, to seabed morphology. In the past decades, significant efforts have been devoted to SPM monitoring in coastal oceans [1–4] and rivers [5–8]. Indeed, the need to quantify SPMs in the water column at various temporal and spatial scales in natural flows has been identified in a large range of industrial (hydroelectric resources management, pelagic resources monitoring, dredging strategies...) and environmental applications (fluvial and coastal morphodynamics, prediction and monitoring of extreme events in oceans and rivers...), which relate to current environmental, social and economic challenges.

Amongst a large number of techniques for measuring SPM [9], acoustics offers a wide range of possibilities. Active acoustics in underwater environments has the advantage of being non-intrusive, and provides measurements along profiles with high temporal and spatial resolutions depending on the selected frequency. In addition, acoustics has benefited from several recent advances both on the theoretical and instrumental frameworks (single and multi-frequency systems) [10–15]. In particular, backscattering models have been designed to describe the intrinsic scattering properties of particles of organic or mineral composition [16]. These models allow to empirically (eg. [17,18]) or theoretically (eg. [19–22]) estimate the intensity backscattered by a single particle placed in a pressure field, for any particle size (or size distribution) and any frequency of the incident pressure field. Given volume backscattering strength measurements at a given frequency, these models allow acoustic inversions to retrieve the volume or mass concentration of a wide range of SPM in the water column, from zooplankton in open oceans and coastal

* Corresponding author at: Laboratoire d'Informatique Signal et Image de la Côte d'Opale, 50, rue Ferdinand Buisson, 62228, Calais, France.

E-mail address: guillaume.fromant@univ-littoral.fr (G. Fromant).

environments, to suspended non-cohesive and cohesive sediment in fluvial, estuarine and coastal environments [17,23–27].

Oceans and rivers are extremely dynamic environments. As such, the content of SPM in the water column can exhibit large fluctuations both spatially and temporally, and at different scales depending on the context (eg. macrotidal estuaries, open ocean internal waves). Thus, SPM content often shows 3-Dimensional variability patterns (eg. [28–32]). Acoustics only deliver a limited information about the content of the water column, as a function of the frequency used. In addition, the measurement is acquired over a finite volume of water. This is the case for Acoustic Backscattering Systems (ABS) [24,33,34], split beam echosounders [35], or single frequency ADCPs [10–14]: they offer a means to retrieve consistent estimates of the SPM concentration over single, horizontal or vertical profiles. Although these acoustic systems are already an improvement for SPM measurements compared to point-wise and intrusive water sampling methods or optical tools, their spatial coverage is still limited. Addressing the physical and biological dynamics of complex areas such as estuaries, near-shore and coastal areas or large rivers often requires time-consuming field operations such as the set-up of observation networks (eg. [28,31,36,37]). In this context, the question of the measurement of SPM dynamics arises, namely: what phenomenon do we want to observe and at what scale is it relevant to measure this phenomenon? With this respect, there is a need to expand the SPM measurements over larger spatial and temporal scales for a more efficient characterization of the distribution and fluxes of SPM, and the associated transport processes.

Although Multi-Beam EchoSounders (MBES) are widely-used among the coastal and fluvial communities [38–40], insonify a large volume of water and thus potentially yield large spatial data coverage, very few studies involve their use for SPM quantification [41–46]. In addition to its primary function of high-resolution sea-floor mapping, MBES technology provides two-dimensional water-column images over the MBES swath. As such, in adding an extra dimension of observation, MBES provide the opportunity to acquire SPM data in the water column with a better representativeness than other acoustic systems typically used for SPM measurements (ABS, ADCP). Yet, the interpretation of the MBES measurements in terms of SPM content is far from being immediate, as data is highly dependent on the antenna beampatterns in emission and reception [47,48]. This results in inconsistencies in the backscattered pressure levels along the MBES fan. Without adequate corrections, these inconsistencies would lead to erroneous values of the Volume Backscattering Strength S_v , from which the mass concentration is derived [16]. The use of MBES as a SPM monitoring tool thus relies on the accurate calibration of each individual beam of the MBES fan, which in practice requires significant resources (financial, material, human) [46,47]. In addition, because it is a single-frequency instrument, the acoustic inversion of MBES data is limited by the prior determination of a mean radius or an Equivalent Spherical Radius (ESR) and by the choice of a backscattering model appropriately describing the acoustical properties of the suspension.

In January 2015, time series of raw Kongsberg EM3002 MBES data at 300 kHz were acquired in the macrotidal estuary of the Aulne River (France). The Aulne River exhibits a high discharge in winter, with SPM concentrations reaching moderate levels around 300 mg/L during discharge events. Concurrently, 4-frequency ABS profiles (Aquascat 1000S–0.5, 1, 2 and 4 MHz), turbidity, salinity and temperature (KOR-EXO) were collected periodically. All the instruments were attached to the same downcasting structure. Concurrent optical measurements identified the fine grain size of the sediments of the river, their aggregation by flocculation, as well as the steadiness of the mean effective density averaged over the size distribution of the observed flocs even though the size distri-

bution was broad [49]. Under these assumptions, a theoretical estimation of the intrinsic backscattering properties of the suspension of interest was devised [49]. A key feature of this theoretical model is to integrate the porosity of the flocs' inner matrices into the backscattering model.

The objective of this work is to assess the possibility to measure absolute spatial and temporal SPM levels in the water column using an MBES calibrated through an original approach. [46] report a successful application of this concept, involving the use of a RESON Seabat 7125 for which each beam was calibrated in a large-scale basin using a suspension of known properties. Instead, the present study proposes a semi-empirical calibration procedure of the MBES deployed from a ship, in calm conditions. The interests in such a technique are numerous: first, it does not imply the use of a large basin in which either a homogeneous suspension or jet of particles of known properties is produced, or individual calibrated hydrophones are used. Second, its realization is fast (half an hour) and can be made *in situ* directly before or after the measurement campaign. This is of particular interest knowing that this kind of calibration must be done regularly to avoid potential systems drifts over time. This field calibration aims at harmonizing the echo levels of the echosounder so that it can deliver absolute volume backscattering strength S_v over its entire fan. S_v are further inverted using an adequate backscattering model, as well as the ESR for the whole suspension estimated from acoustic inversion of independent and simultaneous multi-frequency measurements.

2. Field experiment

2.1. Study site

The experiment was conducted from a small vessel on station under the bridge of Térénez in the Aulne estuary, north-western France (Fig. 1a) in January 21st 2015. The Aulne river estuary is a shallow, macrotidal tributary of the Bay of Brest. Its average discharge is 24 m³/s, with a maximum in February and minimum in August [50,51], carrying approximately 7000 tons of suspended sediment into the Bay of Brest [50] each year. The sediment bed in the estuary is characterized by a combination of sand and silt-mud, with coarser material located downstream. The main minerals in suspension have been identified as phylitic clays, composed of illite, chlorite, kaolinite and micas [50]. The mass concentration of suspended sediment varies seasonally, with highest values observed in winter flood (>1 g/L) and lowest in summer (<30 mg/L). These fine-grained cohesive minerals are subject to flocculation: in suspension they have mostly been observed as small aggregates (microflocs) of diameter <100 μm, although more intense flocculation phases can locally induce the formation of larger aggregates.

2.2. Equipment and survey protocol

The MBES, a Kongsberg EM3002, which operates at a frequency of 300 kHz, was mounted on a pole, deployed from the port side of the R/V Albert Lucas. During over 5 h of sampling during ebb tide, the MBES, recorded >60,000 raw complex backscattered pressure pings with a ping rate of 4 Hz and a fixed pulse-length of 0.15 ms (Fig. 1b). For this particular MBES, the raw backscattered signal arriving at each stave of the sonar receiver antenna was recorded on a SCSI disk. The sample rate was limited to a maximum of 4 Hz due to limitation on the recording speed of the SCSI disk. The range sampling rate of the MBES was set to 15 kHz, leading to 5 cm cell size along the beams (for a corresponding sound velocity of 1500 m/s).

In addition, during the whole experiment, acoustical and optical SPM measurements, as well as physical parameters, were acquired along water column profiles, at regular time intervals (Fig. 1b). The instruments, a multifrequency ABS (Aquascat 1000S, [52]) and a multi-parameters probe (YSI KOR-EXO 1) recording salinity, temperature, pressure and turbidity, were also deployed from the N/O Albert Lucas. They were all attached horizontally to the same weighted downcasting structure, ensuring consistency between the measurements provided by each instrument. 20 casts were carried out at an average downcasting speed of 0.5 m/s. The Aquascat measures the root-mean-square backscattered voltage V_{rms} at 4 frequencies (0.5–1–2–4 MHz) along several cells at each ping. In this experiment, the length of the cells was set to 5 mm so that a total of 256 cells were recorded at each ping. The ping rate was set to 8 Hz and ensemble averages over eight pings were computed. The instrument was placed horizontally on the downcasting frame, so that each ping recorded by the instrument could be associated to one particular depth. Such a procedure has been chosen in case of strong vertical gradient of suspended sediment concentration, potentially causing attenuation effects. Moreover, under a reasonable assumption of weak horizontal gradient in terms of suspended load, proceeding as such permitted further averaging of the acoustic measurements over one ping profile. In the following sections, we also make the reasonable assumption that there was no multiple scattering effects, supposed to appear for SSC higher than 10 g/L [53] (one order of magnitude higher than the peak value observed on site). *In situ* water samples were collected using a heavily weighted Niskin bottle at the same time intervals and at a constant depth of 8 m, in order to convert the turbidity data to Suspended Sediment Concentration (SSC) through a linear relationship described in [49]. A full description of the instrumentation, set up and sampling strategy can be found in [49].

3. Acoustic method for the determination of suspended sediment concentration

3.1. MBES “minimal” calibration

This field, semi-empirical calibration aims at harmonizing the echo levels of the echosounder so that it can deliver absolute volume backscattering strength S_v over its entire fan. The Kongsberg EM3002 MBES has two distinct linear antennas, one serving as

transmitter, the other as receiver. The transmitted signal is wide athwart (insonifying the water column over a swath angle up to 130°) and narrow along (3° azimuthal beamwidth). The backscattered signal is received over the entire swath insonified by the transmitted acoustic pulse on its N elementary stove sensors [54]. Raw acoustic data are then beamformed in order to obtain an image of the acoustic backscattered pressure of the water column. In order to optimize computing time, 81 beams were generated from -60° to 60° with a constant beamspacing of 1.5° .

The beamforming process involves beam steering, which has several inconveniences: introducing differences in echo levels over the entire fan of the MBES (increase or decrease depending on the geometry of the antenna), and widening the equivalent solid angle Ψ as steering angles increase [46,55]. Fig. 2 schematically illustrates these differences, in the case of an idealized linear antenna in both emission and reception (for illustration purposes). These differences prevent the MBES from reading a harmonized value over its entire fan; for instance, in the case of a homogeneous suspension, the backscattered level should be constant over the entire fan of the MBES. In addition, a common constant bias to each beam exists in practice, relating the linear relationship between the absolute sound pressure and the recorded backscattered amplitude at the receiver array. This term is often referred to as K_t in the literature when addressing the problem of acoustic inversion of common ABS devices [17]. Inaccurate estimation of this term prevents the system from recording absolute measurements. Some authors recommend the use of calibration protocols involving the measurement of the response of a single target of known target strength [47] or a homogeneous suspension of known scattering properties [17,46] over each beam of the MBES in order to correct the levels of the echoes. These protocols, although theoretically required to fully calibrate the instruments, are time-consuming and require substantial facilities. Taking a different stand, this work reports on a minimal calibration of the MBES, applicable *in situ*. The proposed protocol first consists in correcting a single beam of the echosounder. The differences in echo levels and equivalent solid angle over the entire fan compared to this beam are then estimated theoretically by computing the beam directivity patterns of the complete antenna. Finally, the echosounder can provide a homogeneous measure of the absolute Volume Backscattering Strength S_v over its entire measurement fan.

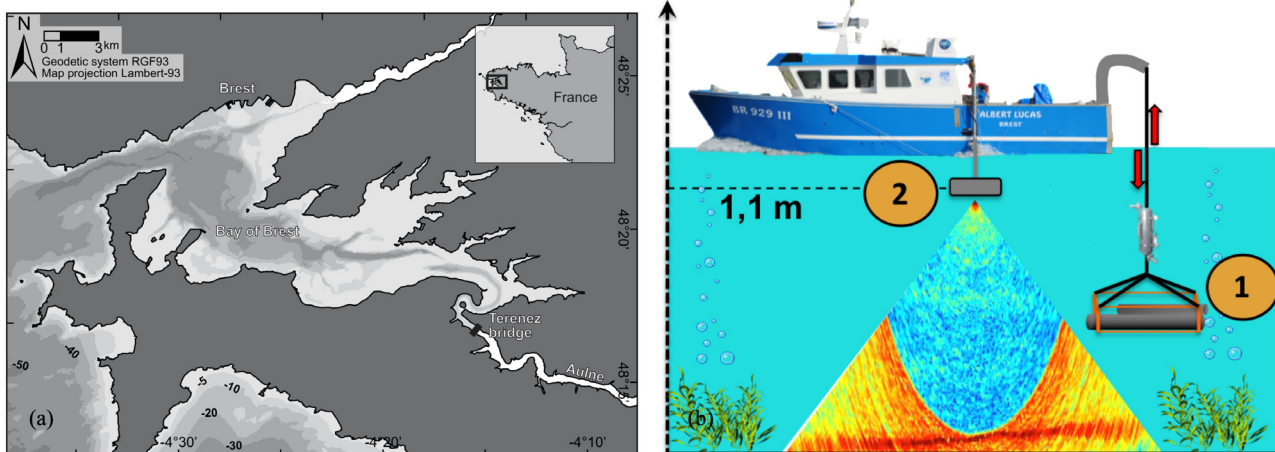


Fig. 1. (a) Aulne estuary location. The Terenez bridge is located at the upstream extremity of the estuary ($48^\circ 16' 07.38''$ N, $4^\circ 15' 48, 43''$ W); (b) Schematics of the sampling protocol carried out at the Terenez bridge: 1/Downcasting frame vertically sampling the water column in terms of temperature, salinity, turbidity (YSI KOR-EXO) and acoustic volume backscattering strength (Aquascat 1000S) at regular time intervals, 2/Kongsberg EM3002 Multibeam Echosounder continuously recording raw acoustic backscatter.

3.2. Constant bias determination

First, the method requires an estimation of the constant bias common to the whole fan of the MBES. This step relies on insonifying a target (Fig. 3a) of known material properties and Target Strength (TS) [56], placing it in one MBES beam denoted c at steering angle θ_c (preferentially close to the central beam). In this case, the target is a 38.1 mm diameter, tungsten carbide sphere, the mechanical properties of which were found in [55]. A specific device was designed to position the sphere under the echosounder (Fig. 3b and c). The sphere was attached to three nylon wires passing inside eye hooks that were attached along the boat (Fig. 3c), allowing the sphere to be moved beneath the echosounder by adjusting the length of the nylon wires. The echosounder was mounted on a pole and deployed from the port side of the ship. The sphere was slowly moved back and forth across the beam of interest, as placing the sphere exactly inside the selected beam was unpractical. The same acquisition parameters (4 Hz ping rate, 0.15 ms pulse length) and processing method (beamforming) are applied for calibration and experimental data, so that the calibration analysis is consistent with the study site dataset. During the calibration measurements, the beam insonifying the target sphere was at $\theta_c = 3^\circ$. A set of >1200 pings was recorded, containing a total of four, slow back and forth crossings of the sphere within the beam of interest. After correcting from spherical spreading and attenuation loss, the object is tracked on the acoustic data. Then the TS values observed by the echosounder are averaged. Finally, the calibration constant is obtained from the difference between the TS measured by the beam under calibration and the theoretical TS of the sphere.

The theoretical scattering properties of the tungsten carbide sphere can be estimated by computing its modal series solution [22,57]. In the far geometric regime (product of wave number k and sphere radius a) such as here, the computed TS presents several quick variations with ka due to interferences between various sphere resonance modes. Given the current measurement conditions we hypothesize that these interferences are likely to be damped (nylon knots and wire running over the target's surface, target motion, natural variability of the surrounding medium such as turbulence. . .). Therefore a high-pass formulation [20] was preferred over the modal series solution, even though it may result in a slight bias. Note that the use of the modal series solution should

however be preferred in standard calibration conditions (i.e. in a test basin). Here the TS of the sphere was found equal to -40.8 dB at 300 kHz using a high-pass formulation (against a value of -38.23 dB using the exact modal series solution).

The advantage of this procedure is that it can be carried out *in situ* provided that there is no high current that may cause the target to drift. For this experiment, an isolated dock in the Brest harbour proved to be a satisfying location in clear water conditions.

3.3. Extension of the calibration to the entire fan of the MBES

The calibration can be extended from the calibrated beam c to the other beams with prior knowledge of the antenna beam patterns, allowing to correct for sensitivity changes and equivalent solid angle variations over the entire fan of the MBES. This step is critical, as such information relative to the design of the antenna is subject to industrial secret. For the present study, Ψ and C_{cal} values were kindly provided by Kongsberg Maritime.

Taking account of the previous hypothesis (Ψ and C_{cal} variation along the MBES fan), S_v can be written as follows [54]:

$$S_v = F_{dB}(\theta_k, t) + 20\log_{10}R + 2\alpha R - C(\theta_k) - 10\log_{10}\left(\Psi(\theta_k)\frac{c\tau}{2}\right) \quad (1)$$

$$C(\theta_k) = C_{abs} + C_{cal}(\theta_k)$$

F_{dB} is the raw acoustic backscattered intensity, obtained just after beamforming. R is the range from the phase centre of the echosounder, α the attenuation coefficient due to water absorption, c the sound velocity in water, τ the pulse length and $C(\theta_k)$ and $\Psi(\theta_k)$ are the echo level correction and "beamwidth factor". $C(\theta_k)$ is decomposed into the sum of the constant bias C_{abs} , corresponding to the echo level correction for the calibrated beam ($C_{cal}(\theta_k = \theta_c) = 0$) and a "calibration factor" $C_{cal}(\theta_k)$, corresponding to the beam sensitivity of each beam. From the measurement of C_{abs} for the beam c , the calibration parameters (calibration and beamwidth factors $C_{cal}(\theta_k)$ and $\Psi(\theta_k)$) of the other beams are obtained by modelling the theoretical beampatterns of the antenna using classical formulas [58]. Modelling the beampatterns requires knowledge of the exact geometry of the antenna (elementary stave dimensions and positions), and if possible a measurement of a sole elementary stave beampattern D_n^{elem} in both emission and recep-

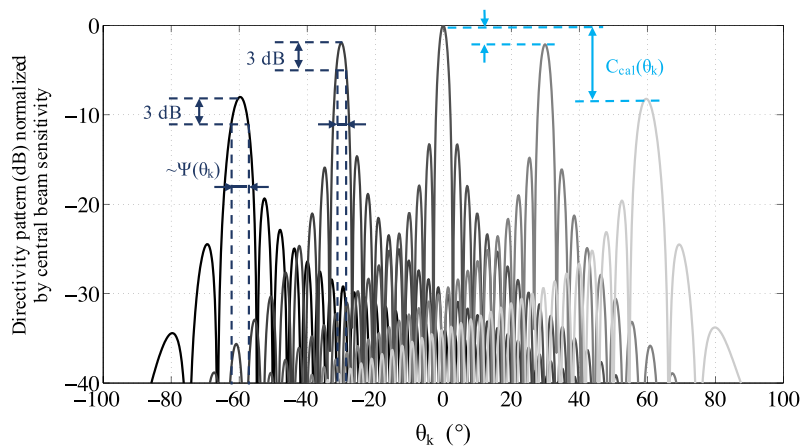


Fig. 2. Directivity patterns of an idealized linear antenna of 80 equidistant spherical staves shown here at five distinct steering angles, ranging from $\theta_k = -60^\circ$ (black) up to $\theta_k = 60^\circ$ (light grey) with 30° increments. All directivity patterns are here normalized with respect to the central beam sensitivity at $\theta_k = 0^\circ$. The diagrams illustrate the decrease of the angular resolution at -3 dB (beam opening), used here as a proxy for the beam equivalent solid angle $\Psi(\theta_k)$, here coupled with a decrease (for an idealized antenna case) of the beam sensitivity $C_{cal}(\theta_k)$ with respect to the beam steering. Data provided in this figure only serve as an illustration for the general antenna beampatterns. The proprietorial C_{cal} and Ψ values of the EM3002 were kindly provided by Kongsberg Maritime. (For interpretation of the references to colour in this figure legend, the reader is referred to the web version of this article.)

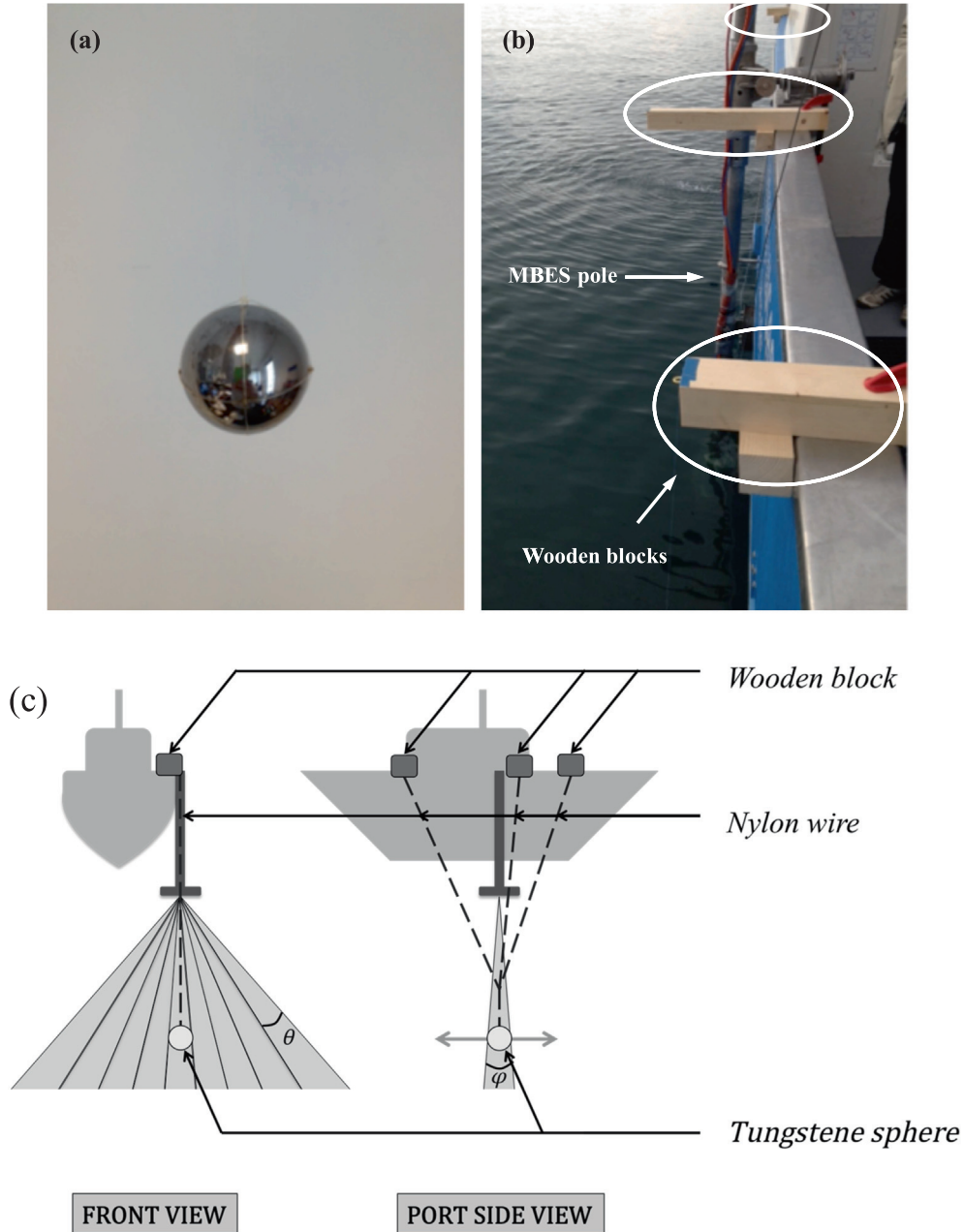


Fig. 3. (a) 38.1 mm tungsten carbide calibration sphere; (b) Photo of the port side of the ship, showing the three wooden blocks from which the nylons wires bearing the sphere are positioned; (c) Schematics of the *in situ* calibration protocol used to calibrate the MBES.

tion. More precisely, considering an antenna of N elementary elements, let $\vec{\rho}_n$ refer to the radial distance of the n^{th} element of the antenna relatively to the origin (for example taken at the edge of the linear antenna), and \vec{u} a unit vector defining the azimuth θ and site φ of any point in space expressed in a spherical coordinate system, the directivity pattern of the whole antenna can be written as follows:

$$D(\theta, \varphi) = \frac{1}{N} \sum_{n=1}^N W(n) D_n^{\text{elem}}(\theta, \varphi) \times e^{j \frac{2\pi}{\lambda} \vec{\rho}_n \cdot \vec{u}} \quad (2)$$

Where $W(n)$ is a Hamming window, used here to lower the secondary lobes levels:

$$W(n) = 0.54 + 0.46 \cos\left(\frac{2\pi n}{N}\right) \quad (3)$$

3.4. Equivalent spherical radii (ESR) estimation using a multifrequency approach

The multifrequency inversion of ABS data yields a numerical density expressed in number/ m^3 (hence a mass concentration) distributed over several input size classes or Equivalent Spherical Radius [49]. In the present section, we present a mean to estimate an ESR for the whole suspension (further referred to as SESR for Suspension Equivalent Spherical Radius) from the multifrequency inversion outputs, information necessary to reduce the number of unknowns of the inverse problem to two (SESR and mass concentration) and further invert the MBES single-frequency measurements.

First, ensemble averaged measurements of Aquascat root-mean-square backscattered voltage V_{rms} were corrected for absorp-

tion, spherical spreading and system-dependent parameters. Even at high frequencies (>0.5 MHz), no noticeable sediment attenuation could be observed. So, attenuation was neglected during the processing of the acoustical data (ABS and MBES). To generate vertical profiles of acoustic backscatter, a mean, measured acoustic backscattered level was obtained for each ping by averaging over the 100 sampling cells centred around 0.5 m, with a pulse length of 6.67 μ s. Backscattered profile values were then converted into volume backscattering coefficients s_ν (related to the volume backscattering strength as $S_\nu = 10\log_{10}(s_\nu)$). Then, the data were inverted using the Non-Negative Least Square algorithm NNLS [59], yielding a numerical density or mass concentration estimate for each input ESR class (16 log-spaced classes ranging from $a_m = 30 \mu\text{m}$ to $a_M = 500 \mu\text{m}$) [49]. The central assumption in the NNLS approach consists in considering that the measured s_ν at each of the four different frequencies ν is the linear combination of the individual contributions of the particles present in the sampled volume.

$$s_\nu(\nu) = \sum_i \sigma_{bs}(a_i, \nu) * N_i M_i = \frac{3}{4} \frac{N_i}{\rho_0 \pi a_i^3} \quad (4)$$

With a_i the ESR of size class i and N_i (M_i) is the numerical density (mass concentration) of particles with an ESR a_i , expressed in number/m³ (kg/m³). The N_i (hence M_i and subsequently the total mass concentration M) are the solution of the multifrequency inversion. The backscattering model (σ_{bs}) used to invert the data is derived from high-pass Sheng & Hay model [53], built under the assumption that the suspended material, taking the shape of small aggregated particles or flocs, possessed backscattering characteristics linked to their averaged inner matrix porosity, supposed constant during the whole experiment [49]:

$$\sigma_{bs} = \frac{a^2}{4} \frac{K_f^2 (ka)^4}{(1 + \varepsilon(ka)^2)^2} \quad (5)$$

$$K_f = \frac{2}{3} \left(\frac{\gamma \zeta^2 - 1}{3\gamma \zeta^2} + \frac{\gamma - 1}{2\gamma + 1} \right)$$

$$\gamma = \frac{\rho_0}{\rho_w}, \zeta = \frac{c_0}{c_w}$$

$$\varepsilon = \frac{K_f \sqrt{2} \gamma \zeta + 1}{2 \gamma \zeta - 1} \quad (6)$$

$$\rho_0 = \Phi \rho_w + (1 - \Phi) \rho_s$$

$$c_0 = \left([\Phi \rho_w + (1 - \Phi) \rho_s] \cdot \left[\frac{\Phi}{\kappa_w} + \frac{1 - \Phi}{\kappa_s} \right] \right)^{-\frac{1}{2}} \quad (7)$$

With Φ the porosity of the aggregates, k the wave number, a the particle radius, ρ_w and κ_w the density and compressibility of the water, and ρ_s and κ_s the density and compressibility of the elementary particles forming the aggregates. ρ_0 and c_0 are respectively the density of the aggregate and Wood's sound speed. γ and ζ are the ratios of density and sound velocity between the particle and the water respectively, and ε a constant set to take the penetrability of the particle in the geometric regime of the model into account [20]. In this particular study, the optimum porosity was set to $\Phi = 0.87$. Complete details on the model used to invert the multifrequency data are contained in [49]. This model has been seen to successfully predict SSC of small estuarine aggregates using the NNLS algorithm.

The SESR is further estimated considering Eq. (4) for a unique size class accounting for the whole suspension, and from which

the backscattered signal (of particles of a single "weighted" size) would equal the backscattered signal of the actual suspension (sum of the acoustical contributions of each particle in size class i). This approach allows the number of unknowns from i size classes to be reduced to two (SESR and Total mass concentration). The formulation is given as follows:

$$s_\nu(\nu) = \sigma_{bs}(A_e, \nu) * N_e \quad (8)$$

$$N_e = \frac{3M}{4\pi A_e^3 \rho_0} \quad (9)$$

Where A_e is the SESR, accounting for the whole suspension, and N_e the numerical density of particles of SESR A_e . The approach comes down to "degrading" the information obtained from the multifrequency inversion through an optimum search of the SESR A_e corresponding to the whole suspension. Naturally, A_e lies in-between the lower (a_m) and upper (a_M) bounds chosen for the input ESR classes. Using Eq. (4), 8 and 9 :

$$A_e = \underset{a_e}{\operatorname{argmin}} \left(\sum_i N_i \sigma_{bs}(a_i, \nu) - N_e \sigma_{bs}(a_e, \nu) \right) \quad (10)$$

Where a_e spans through all size classes in the range $[a_m, a_M]$. The N_i are the outputs of the multifrequency inversion. N_e is linked to the total mass concentration (Eq. (9)) and computed for each a_e step. Further on, ν in Eq. (10) will be set to 300 kHz, the operating frequency of the MBES.

3.5. Single frequency MBES inversion

MBES S_ν measurements are inverted using the previously developed backscattering model and the SESR estimated for the whole suspension from the ABS measurements (Eqs. (8)–(10)).

Data for each beam of the MBES was considered independently, in order to facilitate processing. Each beam was corrected for spherical spreading, sound absorption and applying the angle-dependant calibration coefficients in order to obtain instantaneous s_ν measurements.

Following the assumption of incoherent scattering, the s_ν obtained for a given beam were averaged along the direction of the beam and over time in order to reduce the relative standard error of the backscattered intensities and the subsequent expected error on the mass concentration [60]: a two-dimensional moving average with a moving window of 5 cells along-beam (25 cm length for the central beam, where beam direction matches with the depth dimension) and 60 cells over time (15 s length) was used, so that each backscattered intensity value was an average of 150 samples. Note that no lateral averaging of the backscattered intensities across individual beams has been performed, since both the beamforming step and the calibration procedure consider each beam separately.

A total of 20 ABS profiles were inverted to obtain estimations of the SESR values over the entire duration of the experiment. The SESR data were linearly interpolated throughout the experiment: 1/ over time to fit the ping rate of the MBES (4 Hz) and 2/ according to the beam sampling depths, which vary with the steering angles. Uniform extrapolation was applied to the last bins of the water column when those were empty of data by extending the last non-null bin's value to reach the bottom depth.

4. Results

4.1. Physical parameters

Fig. 4 shows the evolution of Salinity, Temperature and Mass concentration profiles during the whole experiment. The time

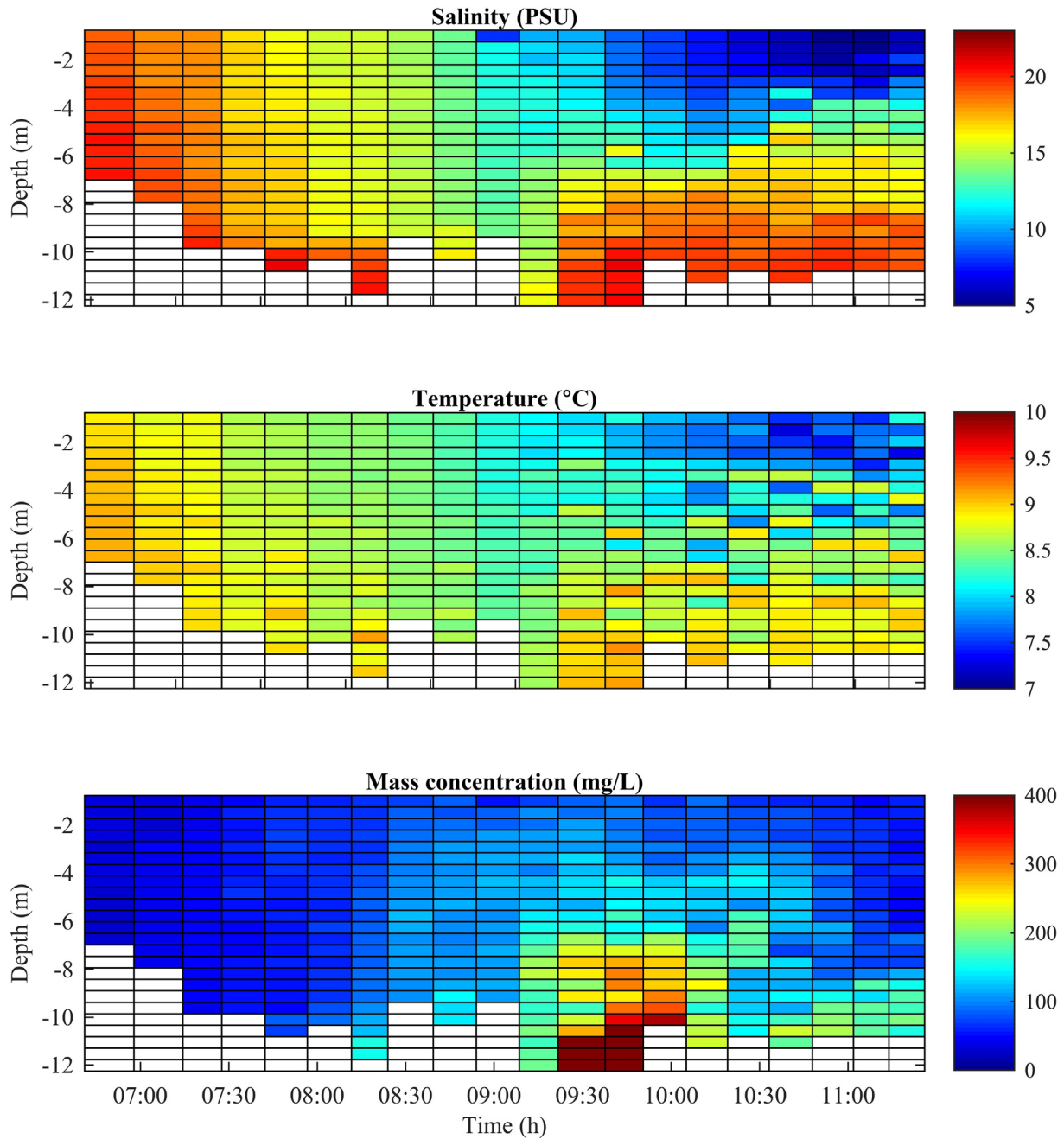


Fig. 4. Physical parameters variation during the experiment, time is in UT. From top to bottom, Salinity (PSU), Temperature (°C) and Mass concentration (mg/L) are displayed. The experiment is marked by vertical discontinuities, and a moderate turbidity event, occurring after mid-tide where the current is the strongest.

lapses between each profile are near to 15 min. The first ten profiles, up to 9:00 am (UT), were hard to achieve due to the presence of a strong current preventing the downcasting structure to reach the bottom of the river.

The vertical structure is marked by its strong salinity gradient. Its position in the water column evolves with the tide, nearly reaching the surface in the end of the experiment. Temperature variations are quite limited in amplitude, decreasing from 9 °C to 7.5 °C. A small temperature gradient appears in the end of the experiment, due to the presence of unmixed fresh water coming from the river after the slack tide. The recorded mass concentra-

tions are characterized by a moderate turbidity event localized in time and depth between 9:15 am and 10:30 am (200–500 mg/L).

4.2. Equivalent spherical radii estimation

Fig. 5a illustrates the NNSL output mass concentration in mg/L for each input ESR class and each depth cell for one profile. Following Eq. (10), the SESR is found for each depth cell and stacked to further be used for the MBES single frequency inversion (Fig. 5b). SESR range from 70 μm to 170 μm and appear to be continuously increasing throughout the experiment. There appears to be no

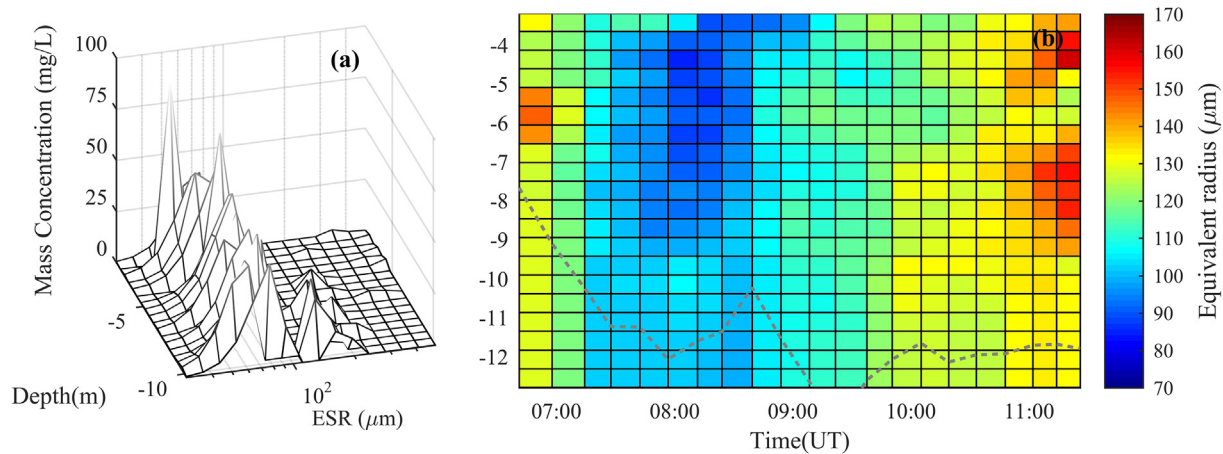


Fig. 5. a) NNLS solution per size class for each sampled depth; b) Suspension equivalent spherical radii (SESR) from the whole experiment. Grey dashed line shows the limit below which SESRs were extrapolated. (For interpretation of the references to colour in this figure legend, the reader is referred to the web version of this article.)

strong vertical stratification of the SESR in the water column. Suspended material are seen to become broader as the tide level decreases.

4.3. MBES backscattered intensity inversion results

Every 81 beam file of the MBES, containing >60,000 pings, was inverted following the steps described in section 3.3. The backscattering cross-section σ_{bs} used for the inversion is the same as for the ABS data. Fig. 6 represents the inverted time series MBES signal for the central beam along the water column, completed with a comparison between two inverted beams at 0° and 30° and the *in situ* observations at a fixed depth of 7.75 m. The blanks in the MBES data (Fig. 6) are the results of sudden system failures (eg. ~ 9:40 AM) that occurred regularly as the SCSI disk stopped recording the raw data. These time-lapses thus correspond to reboots of the system. A first visual inspection of Fig. 6a reveals that the estimated mass concentration continuously grows from the beginning of the experiment (beginning of the ebb, when concentrations were of the order of 50 mg/L) up to approximately 9:30 am. A highly scattering layer can also be observed around 10 m, below which the mass concentration is 1.5 to 2 times larger than above. With the insight given by Fig. 4a, this layer is suspected to coincide with the salinity gradient. After 9:20 am, a moderate turbidity event occurs, with concentrations reaching >600 mg/L. This event is also characterized by a clear vertical concentration gradient that can be seen throughout the water column up to approximately 10:30 am. After 10:30 am, the mass concentration decreases down to 70 mg/L–150 mg/L, still showing a well-marked gradient near the bed. Note that the strong echo visible between 10:30 am and 11:00 am at 7–8 m comes from a turbidity probe deployed for the whole duration of the experiment. Unfortunately, the latter failed during the experiment and no data were recorded.

Fig. 6b presents the concentration time series observed by two beams of the MBES ($\theta_c = 0^\circ$ and $\theta_c = 30^\circ$) at the water sampling depth ($z = 7.75$ m). The spatial pattern of MBES mass concentration estimates and its evolution over time are within a good agreement compared to the actual mass concentration variations determined from water samples. This agreement, which is consistent for most of the beams, is very satisfactory given the relatively high variability of the mass concentration time series (visible on the raw mass concentration time series on Fig. 6b). Note that due to the sampling strategy and the instruments in use, the sampled volumes between the Aquascat and the MBES differed, both qualitatively (~5 m lag

streamwise) and quantitatively (Aquascat volumes are smaller than the MBES volumes). However, the suspended sediment horizontal structures were believed to be sufficiently extensive in the horizontal direction enough so that the assumption that the suspended load was invariant between the two sampling positions at similar depth could be made.

A tendency to localized under- and overestimations of the mass concentration is to be noted, probably as an indicator of the sensitivity induced by the SESR determination, and an expression of natural variability given all the assumptions made for the model generation [49].

As a matter of verification, a comparison between mass concentrations estimated from the ABS and the MBES data (measurements from the central beam, concurrent to the ABS vertical profiles) is also presented (Fig. 7). The MBES (Fig. 6a) and ABS (Fig. 7a) time series display a similar trend, spatially and temporally. Despite the growing dispersion of the results with respect to mass concentration (note the log-scale of Fig. 7b), a clear correlation exists between the ABS and MBES measurements ($R^2 = 0.66$, Fig. 7b). This level of consistency was expected since the MBES mass concentrations were computed using the ABS ESR. On the contrary, natural variability or differences in sampling volumes are thought here to be responsible for the dispersion of the data around the 1:1 line (RMS = 60.83 mg.L⁻¹, Fig. 7b).

Fig. 8 shows the inverted mass concentration on six echograms taken at 6 different instants. A clear contrast can be observed near the riverbed, where a higher concentration layer sets up a little before 9:20 am (UT) from the port side of the echosounder (Fig. 8a), to further completely cover a 2 m height layer above the bed (Fig. 8b) and suddenly disappear a few minutes later (Fig. 8c), to be linked with the moderate turbidity event (see Figs. 4c, 6). It becomes possible to appreciate the slow dynamics of this more turbid layer by looking at several consecutive inverted echograms, showing alternating height decrease/increase of this layer, sometimes revealing 2-Dimensional structures of the concentration field (Fig. 8d and f).

On each echogram of Fig. 8, the previously mentioned turbidity probe (Fig. 6a) can be seen as well at a constant depth of 6 m under the echosounder, on an across-track distance of approximately 5 m.

Some calibration artefacts seem to be visible on the port side (positive across-track distances on Fig. 8) of the echosounder (10° to 30°), where the observed mass concentrations are nearly systematically 25% to 30% higher at a constant elevation compared

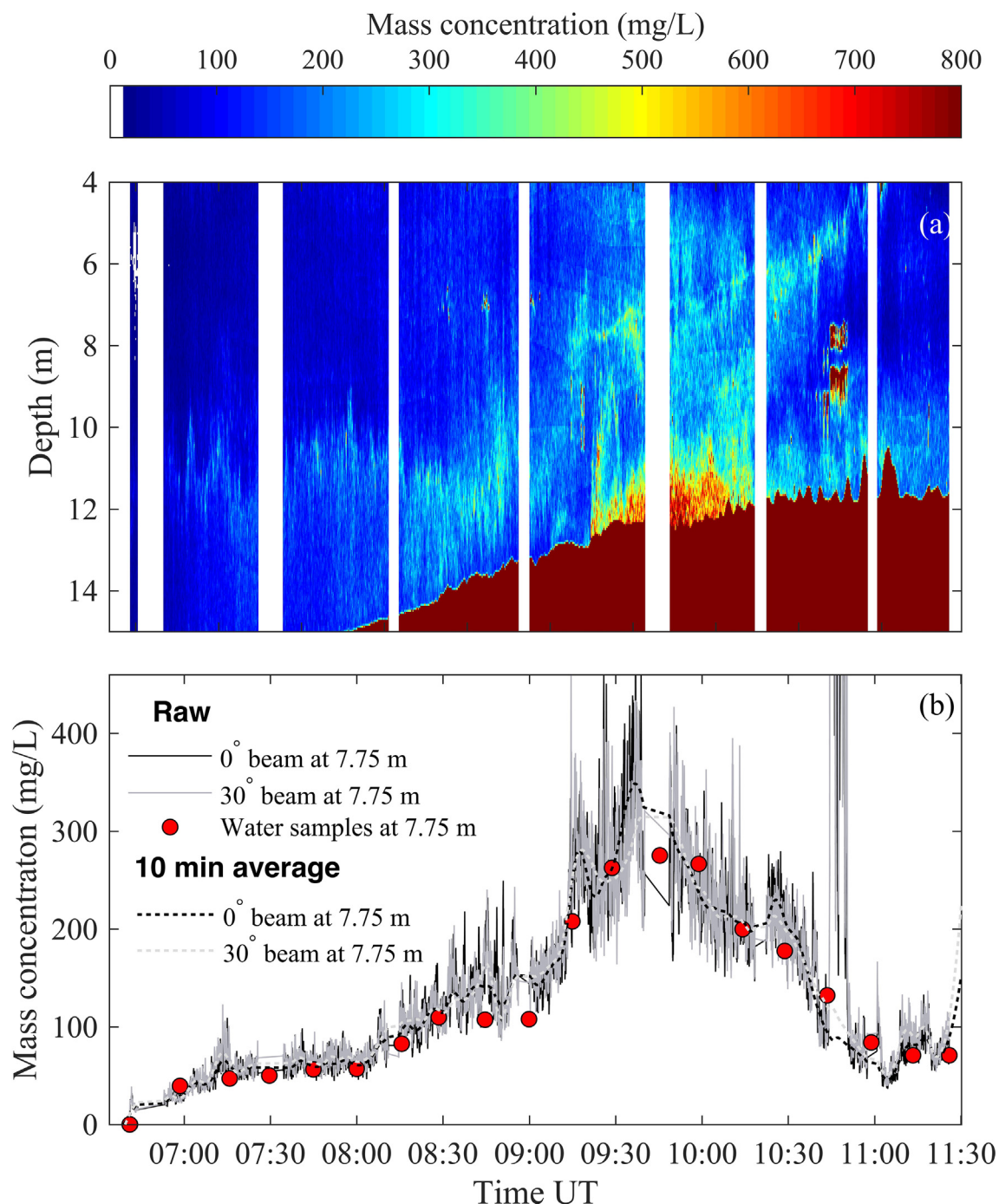


Fig. 6. Top: Inverted mass concentration in mg/L observed from the central beam of the echosounder – white areas correspond to system reboots after fatal failures of the SCSI disk; Bottom: Time series of raw (solid lines) and 10 min averaged (dashed lines) mass concentration estimated by the beam in central position (black lines) and steered at 30° (grey lines) vs. *in situ* sample concentrations (red dots). (For interpretation of the references to colour in this figure legend, the reader is referred to the web version of this article.)

to the starboard side (negative across-track distances on Fig. 8). However, this does not prevent the echograms from returning good insight on the deeper layer concentration field dynamics.

Due to the spatial variability of the suspended sediment load and noise in the MBES data, the raw correlations between the overall inverted MBES concentration estimates (over all beams) and the vertical profiles of *in situ* optical concentrations remain low. The MBES estimated mass concentration signal at each beam was thus low-pass filtered using a moving average with a 10 min window (Fig. 6b) to extract the low frequency variations (smoothing effect

on the concentration time series) and compared to the mass concentrations obtained by the optical data, which were acquired every 15 min along vertical profiles. The results of such a comparison are shown in Fig. 9. The first 6 m of the MBES near field were discarded from the correlation, as well as the last meters of the water column that were not sampled by the optical turbidimeter. [61] reports the nearfield extends of the EM3002 to approximately 7 m, yet echo strength measurements become quite stable after 5 to 6 m. Fig. 9a shows the coefficient of determination of the comparison between inverted mass-concentrations at each beam and

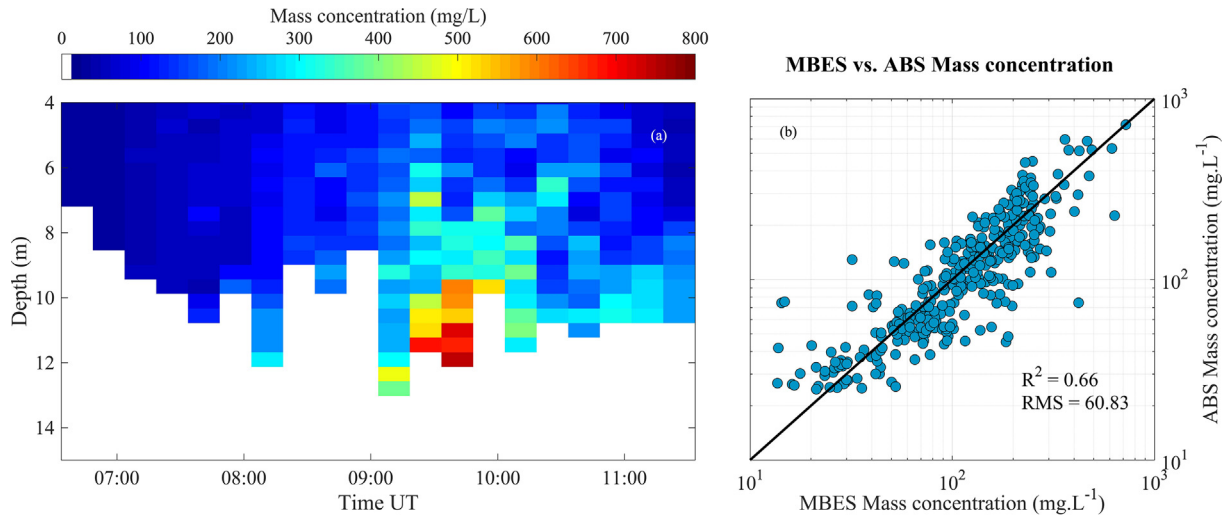


Fig. 7. (a) (b) Inverted mass concentration in mg/L observed from the ABS profiles; (b) Scatter plot of the mass concentrations (mg/L) estimated by the MBES and the mass concentrations estimated by the ABS. The linear regression between the two estimates was forced through the zero crossing of both variables. The coefficient of determination R^2 and root-mean-square RMS are given with respect to the $y = x$ line.

the optically derived mass concentration from 6 m to the deepest depth sampled by the optical turbidimeter. In the ranges $[-20^\circ$ to $+10^\circ$] and $[+30^\circ$ to $+60^\circ]$, the correlation appears satisfactory ($R^2 > 0.6$, $RMS \approx 50$ mg/L), whereas in the ranges $[-60^\circ$ to $-30^\circ]$ and $[+10^\circ$ to $+30^\circ]$, severe drops of correlations appear ($R^2 < 0.3$, $RMS \approx 60$ mg/L). Fig. 9b to h represent the actual scatterplot of MBES estimated mass concentrations (for 7 beams comprised between -30° and $+30^\circ$ with 10° increments) vs the optically estimated mass concentrations, revealing the relative good trend for most of the central beams from -10° to 10° , and satisfactory

results for the beams between -30° up to 10° and 30° to 60° . For the negatively steered outer beams, in the range $[-60^\circ$ to $-40^\circ]$, the observed drop of correlation ($R^2 < 0.2$) is due to a systematic strong underestimation (up to a factor 2) of the mass concentration after the acoustic inversion. To the contrary, the inverted concentrations in the range $[+10^\circ$ to $+30^\circ]$ do present a tendency to systematically overestimate the mass concentration up to a factor 1.5 ($R^2 < 0.5$, see Fig. 8h). The deviations observed in the ranges $[-60^\circ$ to $-40^\circ]$ and $[+10^\circ$ to $+30^\circ]$ are thought to be the result of poor calibration accuracy. The same trends (sectorial underestima-

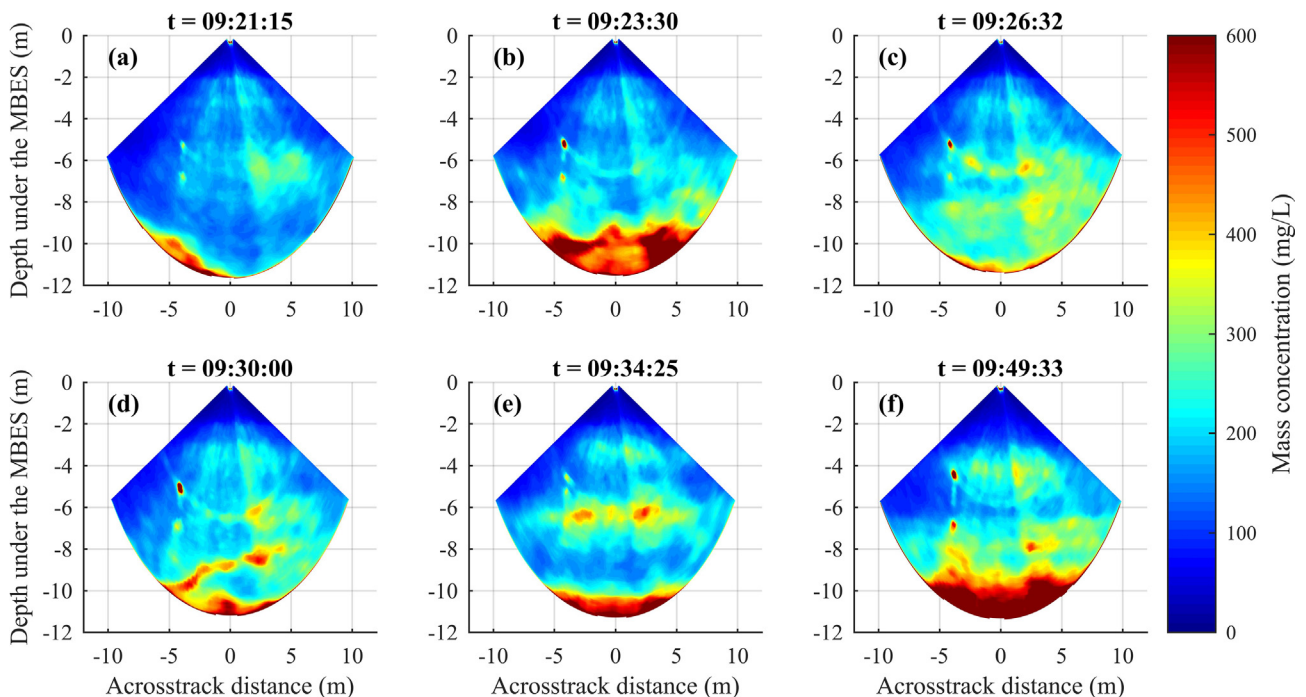


Fig. 8. Mass concentration echograms of six different instants centred around the moderate turbidity event observed during the experiment between 9:20 am and 9:50 am (UT).

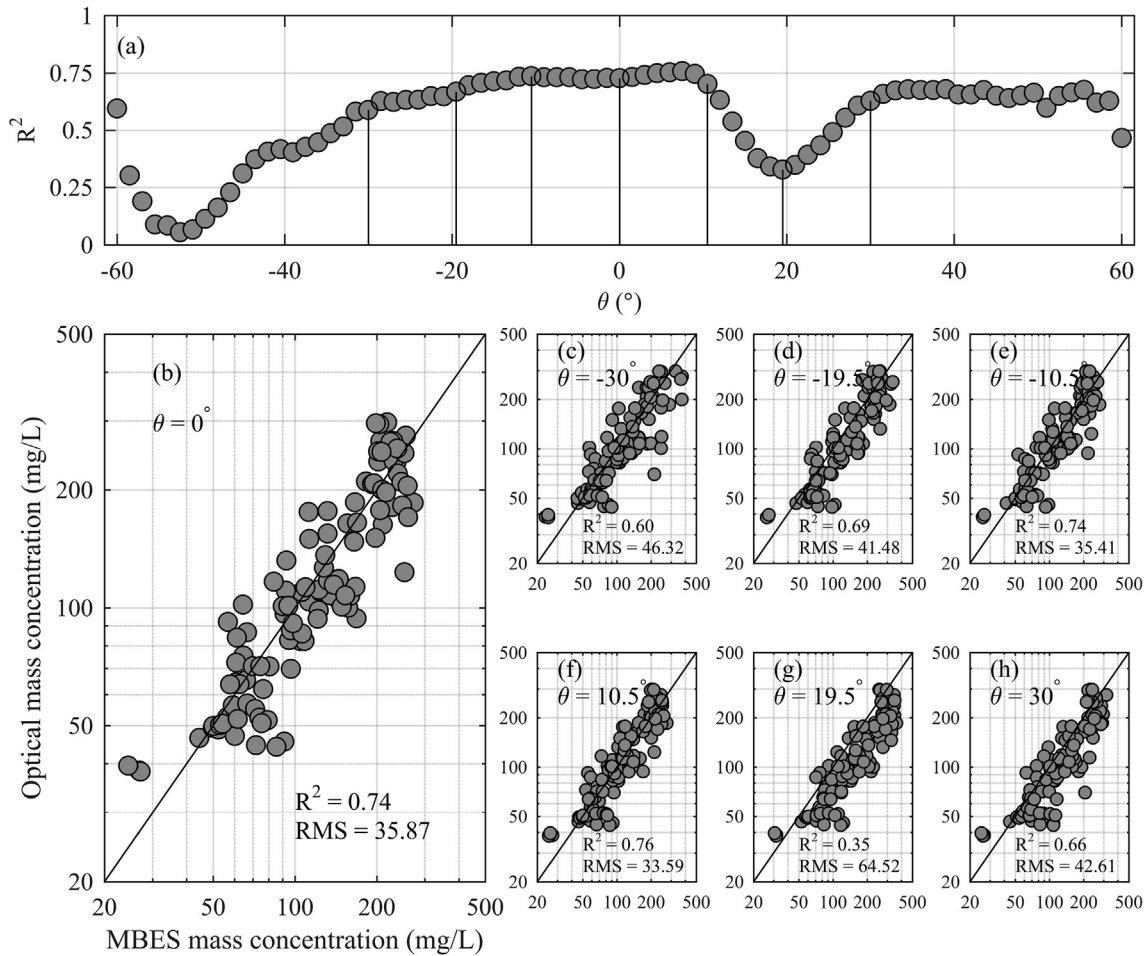


Fig. 9. Scatter plot of the mass concentrations (mg/L) estimated by the MBES and the mass concentrations obtained through optical measurements. The linear regression between the two estimates was forced through the zero crossing of both variables. The coefficient of determination R^2 with respect to the $y = x$ line is given.

tion between -60° and -40° and overestimation between $+10^\circ$ and $+30^\circ$) are also visible in the echograms plotted on Fig. 8.

5. Discussion

In situ acoustic signal from aggregated particles in a macrotidal estuary was inverted using a combination of calibrated MBES data acquired continuously with a 300 kHz system and multifrequency observations with limited spatial coverage. Thanks to the reduction of the inverse problem addressed in this study to only two unknowns (SESR + mass concentration), the proposed method has shown success in estimating the two-dimensional field of cohesive sediment concentration in the water column, revealing the 2D spatial patterns of suspended matter under the MBES over time. The correlation between the mass concentration observed by both the turbidimeter and the inverted MBES backscatter data is high ($R^2 > 0.6$) over most of the MBES fan, when considering the low-frequency component of the mass concentration evolution over time during the studied ebb period, as recorded by the optical turbidimeter. The method presented here is promising for applications to the continuous monitoring of suspended particulate matter using a MBES. Other potential applications would require additional development to adapt the backscattering model, such as for coarse sand suspension, which heuristically-based backscattering model is well documented [17], as well as organic particle (eg. Zooplankton) biovolume estimation.

An original calibration has been presented in the present article, involving the empirical calibration of a single beam of the MBES using a standard target, followed by a theoretical spreading of the correction over the entire fan of the echosounder given the measured directivity patterns of the stave elements in both emission and reception, and the antenna geometries. This approach supposes that each stave possesses similar directivity patterns, which might not be accurate in practice. So, the exact directivity patterns of the antenna might not exactly correspond to the ones determined here in a semi-theoretical manner. This is especially true for the high steering angles, potentially leading to systematic errors that can reach up to ± 1 dB, and thus bias the final concentration estimate by a factor of up to 2. However, it would be possible to compensate those effects by empirically tuning for each beam the previously determined C_{cal} values (Eq. (1)), using MBES backscatter measurements acquired while insonifying a sufficiently homogeneous suspension. Finally, using smaller targets, with TS in a range where $ka < 10$, would make the calibration protocol more robust because in that lower range of ka values, the ambiguity on the TS value due to interferences of modes of sphere resonance disappears in the modal series solution. The use of the TS resulting from the exact modal series solution for the tungsten carbide calibration sphere indeed resulted in constant overestimation of the final estimate by a factor 1.5 to 2. The calibration proposed here for the MBES remains a *minimal* calibration, which still offers the advantage of being straightforward and easy to reproduce, as well as an opportunity to reduce operational costs.

In particular, it has proven to be successful in the present study on wide sectors of the present multibeam fan, $[-30^\circ$ to $+10^\circ]$ and $[+30^\circ$ to $+60^\circ]$ ($R^2 > 0.6$).

The backscattering model used in this case study is considered to be adequate, even if some misfits exist on the final mass concentration estimated through multifrequency inversion. Discrepancies are likely due to a misattribution of the NNLS solution in the selected size classes [49]. Such a misattribution of the solution is expected to cause deviations in the ESR determination [24], thus ultimately leading to over or underestimations of the concentration obtained after the MBES single frequency inversion. This part of the method is also the most sensitive, as the backscattering cross-section varies according to a^6 in the Rayleigh regime. In addition, the absorption by suspended aggregates was neglected in this hydro-sedimentary context of the present case study, as its effects were not noticed on the ABS data [49]. This may be incorrect for deeper layers (≈ 11 m), which were not systematically sampled by the instrument.

The resulting uncertainty on the concentration estimate thus strongly relies on our capability to describe the scattering properties of the suspension and the robustness of the instrumental calibration procedure. To date, an uncertainty as low as 50% on the final estimate of the concentration is seldom reached due to the numerous assumptions made throughout the processing chain, more specifically for natural suspensions such as estuarine aggregates [62,63].

The present study underlines how intricate the resolution of the inverse problem can be in practice. Eq. (4) has as many unknowns as size classes. This prompts a prior estimation of the size distribution or at least ESR distribution, to then estimate the mass concentration. Applied to the quantification of suspended sediments, with typical radii ranging from a few microns to a few hundreds of microns, the size determination step requires the use of rather high frequencies ranging from 500 kHz up to 5 MHz. However, the attenuation of acoustic energy increases rapidly with frequency, therefore limiting the useful range and spatial coverage of the instrument. On the contrary, using lower frequencies allows high spatial coverage and thus good representativeness. In the present study, the combination of both higher ($O(\text{MHz})$) and lower frequencies ($O(\text{kHz})$) is shown to be successful to estimate the SSC field. Note however that the problem would have become more complex, if attenuation effects due to viscous friction and/or scattering had manifested, as Eq. (4) would have become implicit.

The ability to obtain mass concentration measurements with an extended coverage offers numerous possibilities to tackle research and applied problems where the quantification of suspended sediment fluxes is needed. For instance, combining novel field observations of accurate suspended sediment concentration over a wide spatial domain, with typical usual high-resolution bathymetric surveys would enhance our capability to characterize large structures such as river plumes, or turbidity currents [64]. Spatially extensive measurements of suspended sediment concentration would also be helpful for the validation of large-scale 3D hydro-sedimentary models, which have been rather poorly constrained due to the difficulties in covering sufficiently wide areas with sufficiently high temporal resolution. In addition, the availability of the MBES raw backscatter data remains rare due to the non-disclosure of sonar characteristics by the manufacturers. This issue is key to disseminate the use of MBES as a continuous SPM monitoring tool. Besides scientific applications, spatially extensive SPM monitoring could be integrated to decision support tools in this context of hydro-sedimentary dynamics, as an addition to bathymetric and seafloor characterization surveys.

Finally, given the strong interest in acoustical methods for continuous monitoring of suspended matter over wide ranges, contin-

ued efforts are required to further reduce the uncertainties on mass concentration estimates. For instance, novel heuristic models describing the scattering properties of different types of natural suspensions are sought out. The approach presented here constitutes a step towards this goal.

6. Conclusions

This work is one of the first inversion of raw MBES data for the purpose of suspended sediment quantification. We confirm the clear potential of MBES to quantify SPM, provided that a model describing the scattering properties of the target suspension is known. Here, *in situ* acoustic signal backscattered from aggregated particles in a macrotidal estuary was inverted using a combination of calibrated MBES data acquired continuously with a 300 kHz system and multifrequency observations at 0.5 MHz, 1 MHz, 2 MHz and 4 MHz with limited spatial coverage. The method described here starts with the determination of an Equivalent Spherical Radius of the suspension through multifrequency inversion involving the use of a suitable backscattering model [49]. The estimated ESR are then used to recover an absolute estimation of the concentration using the single-frequency signal of the MBES, for which a semi-empirical calibration is proposed in order to retrieve readings of the volume backscattering strength over its entire fan. The inversion results are in good agreement with the *in situ* mass concentration, and give access to the temporal evolution of the 2-Dimensional field of mass concentration. This study confirms the interest for the use of active acoustics for SPM monitoring purposes, but also highlights the sensitivity of the acoustic inversion pipeline, and particularly of the sonar calibration protocol and the backscattering model definition. We underline as well the need for continued efforts regarding the characterization of the acoustic properties of natural suspensions, to improve the currently available inversion schemes.

The ability of MBES to collect swath measurements in hull-mounted configuration is key to retrieve large-scale information about the SPM distribution in the water column. The addition of another dimension of observation would clearly bring new insight on SPM monitoring, and would importantly contribute to large-scale suspended sediment dynamics studies.

Declaration of Competing Interest

The authors declare that they have no known competing financial interests or personal relationships that could have appeared to influence the work reported in this paper.

Acknowledgments

This work was conducted in the framework of the ANR EPURE project (Grant 11 CEPL 005 02). This work was also supported by the Laboratoire d'Excellence LabexMER (ANR-10-LABX-19) and co-funded by a grant from the French government under the program Investissements d'Avenir. Contributions from Romain Cancouët, Christophe Martin, Olivier Blanpain, Susanne Moskalsky, Paul Juby and Marcaurelio Franzetti were key to the success of the field measurements. The authors thank the Direction Générale de l'Armement (DGA), the Centre National de la Recherche Scientifique (CNRS), and l'Université de Bretagne Occidentale (UBO) for funding G.F.'s doctorate. The authors would also like to thank the Institut de la Recherche pour le Développement (IRD) for the use of their instruments and datasets, and for the help and support of IRD staff both in the office and at sea. Last but not least, we thank the Pôle Image team and the R/V Albert Lucas crew for their effective cooperation and support during the field campaigns, with

particular attention to Franck Quéré, Alban De Araujo, and Daniel Morigeon.

References

- [1] Odermatt D, Gitelson A, Brando VE, Schaeppman M. Review of constituent retrieval in optically deep and complex waters from satellite imagery. *Remote Sens Environ* 2012;118:116–26. <https://doi.org/10.1016/j.rse.2011.11.013>.
- [2] Thorne PD, Hurther D. An overview on the use of backscattered sound for measuring suspended particle size and concentration profiles in non-cohesive inorganic sediment transport studies. *Cont Shelf Res* 2014;73:97–118.
- [3] Anglès S, Jordi A, Garcés E, Masó M, Basterretxea G. High-resolution spatio-temporal distribution of a coastal phytoplankton bloom using laser in situ scattering and transmissometry (LISST). *Harmful Algae* 2008;7(6):808–16. <https://doi.org/10.1016/j.hal.2008.04.004>.
- [4] Lezama-Ochoa A, Ballón M, Woillez M, Grados D, Irigoien X, Bertrand A. Spatial patterns and scale-dependent relationships between macrozooplankton and fish in the Bay of Biscay: An acoustic study. *Mar Ecol Prog Ser* 2011;439:151–68. <https://doi.org/10.3354/meps09318>.
- [5] Hoitink AJF, Hoekstra P. Observations of suspended sediment from ADCP and OBS measurements in a mud-dominated environment. *Coast Eng* 2005;52(2):103–18.
- [6] Dinehart RL, Burau JR. Repeated surveys by acoustic Doppler current profiler for flow and sediment dynamics in a tidal river. *J Hydrol* 2005;314(1–4):1–21.
- [7] Hoitink AJF, Buschman FA, Vermeulen B. Continuous measurements of discharge from a horizontal acoustic Doppler current profiler in a tidal river. *Water Resour Res* 2009;45:1–13. <https://doi.org/10.1029/2009WR007791>.
- [8] Moore SA, Le Coz J, Hurther D, Paquier A. On the application of horizontal ADCPs to suspended sediment transport surveys in rivers. *Cont Shelf Res* 2012;46:50–63. <https://doi.org/10.1016/j.csr.2011.10.013>.
- [9] Gray JR, Gartner JW, Anderson CW, Fisk GG, Glysson GD, Gooding DJ, et al. Surrogate technologies for monitoring suspended sediment transport in rivers. *Sedimentol Aqueous Syst* 2010:1–45.
- [10] Merckelbach LM. A model for high-frequency acoustic Doppler current profiler backscatter from suspended sediment in strong currents. *Cont Shelf Res* 2006;26(11):1316–35.
- [11] Postel L, da Silva AJ, Mohrholz V, Lass H-U. Zooplankton biomass variability off Angola and Namibia investigated by a lowered ADCP and net sampling. *J Mar Syst* 2007;68(1–2):143–66. <https://doi.org/10.1016/j.imarsys.2006.11.005>.
- [12] Tessier C, Le Hir P, Lurton X, Castaing P. Estimation de la matrice des acoustiques à effet Doppler (ADCP). *Comptes Rendus Geosci* 2008;340(1):57–67.
- [13] Jourdin F, Tessier C, Le Hir P, Verney R, Lunven M, Loyer S, et al. Dual-frequency ADCPs measuring turbidity. *Geo-Marine Lett* 2014;34:381–97.
- [14] La HS, Ha HK, Kang CY, Wählin A, K, Shin HC. Acoustic backscatter observations with implications for seasonal and vertical migrations of zooplankton and nekton in the Amundsen shelf (Antarctica). *Estuar Coast Shelf Sci* 2015;152:124–33. [10.1016/j.ecss.2014.11.020](https://doi.org/10.1016/j.ecss.2014.11.020).
- [15] Trenkel VM, Mazaauric V, Berger L. The new fisheries multibeam echosounder ME70: Description and expected contribution to fisheries research. *ICES J Mar Sci* 2008;65:645–55. <https://doi.org/10.1093/icesjms/fsn051>.
- [16] Medwin H, Clay CS. *Fundamentals of Acoustical Oceanography*. 1997.
- [17] Thorne PD, Hanes DM. A review of acoustic measurement of small-scale sediment processes. *Cont Shelf Res* 2002;22(4):603–32.
- [18] Thorne PD, Meral R. Formulations for the scattering properties of suspended sandy sediments for use in the application of acoustics to sediment transport processes. *Cont Shelf Res* 2008;28(2):309–17. <https://doi.org/10.1016/j.csr.2007.08.002>.
- [19] Morse PM, Ingard AU. *Theoretical Acoustics*. Princeton U. 1986.
- [20] Stanton TK. Simple approximate formulas for backscattering of sound by spherical and elongated objects. *J Acoust Soc Am* 1989;86(4):1499–510.
- [21] Stanton TK, Chu D. Review and recommendations for the modelling of acoustic scattering by fluid-like elongated zooplankton : euphausiids and copepods. *J Mar Sci* 2000:793–807.
- [22] Gaunard GC, Überall H. RST analysis of monostatic and bistatic acoustic echoes from an elastic sphere. *J Acoust Soc Am* 1983;73(1):1–12.
- [23] Greenlaw CF, Johnson RK. Multiple-frequency Acoustical Estimation. *Biol Oceanogr* 1983;2:227–52.
- [24] Holliday DV, Pieper RE. Bioacoustical oceanography at high frequencies. *ICES J Mar Sci* 1995;52:279–96.
- [25] Cox MJ, Letessier TB, Brierley AS. Zooplankton and micronekton biovolume at the Mid-Atlantic Ridge and Charlie-Gibbs Fracture Zone estimated by multi-frequency acoustic survey. *Deep Res Part II Top Stud Oceanogr* 2013;98:269–78. <https://doi.org/10.1016/j.dsr.2013.07.020>.
- [26] Thorne PD, MacDonald IT, Vincent CE. Modelling acoustic scattering by suspended flocculating sediments. *Cont Shelf Res* 2014;88:81–91. <https://doi.org/10.1016/j.csr.2014.07.003>.
- [27] Topping DJ, Wright SA, Melis TS, Rubin DM. High-resolution measurements of suspended-sediment concentration and grain size in the Colorado River in Grand Canyon using a multi-frequency acoustic system. *Proc. 10th Int. Symp. River Sediment.*, vol. 3, 2007.
- [28] Traykovski P, Wiberg PL, Geyer WR. Observations and modeling of wave-supported sediment gravity flows on the Po prodelta and comparison to prior observations from the Eel shelf. *Cont Shelf Res* 2007;27(3–4):375–99.
- [29] Lawson GL, Wiebe PH, Ashjian CJ, Stanton TK. Euphausiid distribution along the Western Antarctic Peninsula-Part B: Distribution of euphausiid aggregations and biomass, and associations with environmental features. *Deep Res Part II Top Stud Oceanogr* 2008;55(3–4):432–54. <https://doi.org/10.1016/j.dsr.2007.11.014>.
- [30] Warrick JA, Xu J, Noble MA, Lee HJ. Rapid formation of hyperpynal sediment gravity currents offshore of a semi-arid California river. *Cont Shelf Res* 2008;28(8):991–1009. <https://doi.org/10.1016/j.csr.2007.11.002>.
- [31] Seers BM, Shears NT. Spatio-temporal patterns in coastal turbidity – Long-term trends and drivers of variation across an estuarine-open coast gradient. *Estuar Coast Shelf Sci* 2015;154:137–51. <https://doi.org/10.1016/j.ecss.2014.12.018>.
- [32] Jiang S, Dickey TD, Steinberg DK, Madin LP. Temporal variability of zooplankton biomass from ADCP backscatter time series data at the Bermuda Testbed Mooring site. *Deep Res Part I Oceanogr Res Pap* 2007;54(4):608–36. <https://doi.org/10.1016/j.dsr.2006.12.011>.
- [33] Holliday D V. Use of acoustic frequency diversity for marine biological measurements. In: Caspers H, editor. *Adv. Concepts Ocean Meas. Mar. Biol. Ed. by Ferdinand P. Diem. F. John Vernberg, Donna Z. Mirkes. – Belle W. Baruch Libr. Mar. Sci. Number 10. – 572 pp. Columbia SC Univ. South Carolina Press 1980. ISBN 0, vol. 66, Akademie Verlag, Berlin; 1981, p. 423–60. 10.1002/iroh.19810660314*.
- [34] Moate BD, Thorne PD, Cooke RD. Field deployment and evaluation of a prototype autonomous two dimensional acoustic backscatter instrument: The Bedform And Suspended Sediment Imager (BASSI). *Cont Shelf Res* 2016;112:78–91.
- [35] Lawson GL, Wiebe PH, Stanton TK, Ashjian CJ. Euphausiid distribution along the Western Antarctic Peninsula—Part A: Development of robust multi-frequency acoustic techniques to identify euphausiid aggregations and quantify euphausiid size, abundance, and biomass. *Deep Sea Res Part II Top Stud Oceanogr* 2008;55(3–4):412–31.
- [36] Pau M, Hammer T. Sediment mapping and long-term monitoring of currents and sediment fluxes in pockmarks in the Oslofjord, Norway. *Mar Geol* 2013;346:262–73. <https://doi.org/10.1016/j.margeo.2013.09.012>.
- [37] Gong W, Jia L, Shen J, Liu JT. Sediment transport in response to changes in river discharge and tidal mixing in a funnel-shaped micro-tidal estuary. *Cont Shelf Res* 2014;76:89–107. <https://doi.org/10.1016/j.csr.2014.01.006>.
- [38] Franzetti M, Le Roy P, Delacourt C, Garlan T, Cancouët R, Sukhovich A, et al. Giant dune morphologies and dynamics in a deep continental shelf environment: example of the banc du four (Western Brittany, France). *Mar Geol* 2013;346:17–30.
- [39] Guillard J, Brehmer P, Colon M, Guennégan Y. Three dimensional characteristics of young-of-year pelagic fish schools in lake. *Aquat Living Resour* 2006;19(2):115–22.
- [40] Colbo K, Ross T, Brown C, Weber T. A review of oceanographic applications of water column data from multibeam echosounders. *Estuar Coast Shelf Sci* 2014;145:41–56. <https://doi.org/10.1016/j.ecss.2014.04.002>.
- [41] Simmons SM, Parsons DR, Best JL, Orfeo O, Lane SN, Kostaschuk R, et al. Monitoring suspended sediment dynamics using MBES. *J Hydraul Eng* 2010;136(1):45–9.
- [42] O'Neill FG, Simmons SM, Parsons DR, Best JL, Copland PJ, Armstrong F, et al. Monitoring the generation and evolution of the sediment plume behind towed fishing gears using a multibeam echosounder. *ICES J Mar Sci* 2013;70(4):892–903. <https://doi.org/10.1093/icesjms/fst051>.
- [43] Cox MJ, Demer DA, Warren JD, Cutter GR, Brierley AS. Multibeam echosounder observations reveal interactions between Antarctic krill and air-breathing predators. *Mar Ecol Prog Ser* 2009;378:199–209.
- [44] De Robertis A. Small-scale spatial distribution of the euphausiid *Euphausia pacifica* and overlap with planktivorous fishes. *J Plankton Res* 2002;24:1207–20.
- [45] Chauchat J, Guillou S, Nguyen KD. Simulation de la sédimentation d'une suspension de sphères par un modèle diphasique. 41eme Colloq. Annu. du Groupe Français Rhéologie 2006:79–82.
- [46] Simmons SM, Parsons DR, Best JL, Oberg KA, Czuba JA, Keevil GM. An evaluation of the use of a multibeam echo-sounder for observations of suspended sediment. *Appl Acoust* 2017;126:81–90.
- [47] Foote KG, Chu D, Hammar TR, Baldwin KC, Mayer LA, Hufnagle LC, et al. Protocols for calibrating multibeam sonar. *J Acoust Soc Am* 2005;117(4):2013–27.
- [48] Gurshin CWD. The use of multibeam and split-beam echo sounders for assessing biomass and distribution of spring-spawning Atlantic cod in the Gulf of Maine. University of New Hampshire; 2012.
- [49] Fromant G, Floc'h F, Lebourges-Dhaussy A, Jourdin F, Perrot Y, Le Dantec N, et al. In Situ Quantification of the Suspended Load of Estuarine Aggregates from Multifrequency Acoustic Inversions. *J Atmos Ocean Technol* 2017;34:1625–43.
- [50] Bassoulet P. *These De Doctorat. Brest: Université de Bretagne Occidentale; 1979*.
- [51] Allen HE, Hall RH, Brisbin TD. Metal speciation. Effects on aquatic toxicity. *Environ Sci Technol* 1980;14(4):441–3. <https://doi.org/10.1021/es60164a002>.
- [52] Aquatec Group Limited (2006). AQUAScat 1000 Acoustic Backscatter System Data Sheet n.d.
- [53] Sheng J, Hay AE. An examination of the spherical scatterer approximation in aqueous suspensions of sand. *J Acoust Soc Am* 1988;83(2):598–610.
- [54] Lurton X. *An introduction to underwater acoustics: principles and applications*. Springer Science & Business Media; 2002.

- [55] Lurton X. Modelling of the sound field radiated by multibeam echosounders for acoustical impact assessment. *Appl Acoust* 2016;101(2):201–21.
- [56] MacLennan DN. Target strength measurements on metal spheres. Marine Laboratory: Librarian Department of Agriculture and Fisheries for Scotland; 1982.
- [57] Faran JJ. Sound scattering by Solid Cylinders and Spheres. *J Acoust Soc Am* 1951;23(4):405–18.
- [58] Marage J-P, Mori Y. *Sonars and Underwater Acoustics*. 1st ed. 2010.
- [59] Lawson CL, Hanson RJ. *Solving Least square problems*. New-Jersey: Prentice-Hall 1974. <https://doi.org/10.1137/1.9781611971217.fm>.
- [60] Betteridge KFE, Thorne PD, Cooke RD. Calibrating multi-frequency acoustic backscatter systems for studying near-bed suspended sediment transport processes. *Cont Shelf Res* 2008;28(2):227–35. <https://doi.org/10.1016/j.csr.2007.07.007>.
- [61] Nilsen KE. Signal processing in EM3002. Forum EM Multibeam Exp. (FEMME), Kongsb. Marit. Users Conf. 2007.
- [62] Navratil O, Esteves M, Legout C, Gratiot N, Nemery J, Willmore S, et al. Global uncertainty analysis of suspended sediment monitoring using turbidimeter in a small mountainous river catchment. *J Hydrol* 2011;398(3–4):246–59.
- [63] McMillan H, Freer J, Pappenberger F, Krueger T, Clark M. Impacts of uncertain river flow data on rainfall-runoff model calibration and discharge predictions. *Hydrol Process* 2010;24:1270–84.
- [64] Clarke FEH. First wide-angle view of channelized turbidity currents links migrating cyclic steps to flow characteristics. *Nature Communication* 2016;7(1):1–13. <https://doi.org/10.1038/ncomms11896>.